SUPPLEMENTARY INFORMATION

Enhanced ultrafast cubic nonlinearity in the carbazole-picric acid complex for potential applications in photonic devices: Kerr nonlinearity with two-photon absorption

Mohd Mehkoom[1], Farman Ali[2], Amit K. Pradhan[3], Prasanta K. Datta[3], Umakanta Tripathy[1$]*

[1]Department of Physics, Indian Institute of Technology (Indian School of Mines) Dhanbad, Dhanbad-826004, Jharkhand, India

[2]Department of Applied Chemistry, Faculty of Engineering and Technology, Aligarh Muslim University, Aligarh-202002, India

[3]Department of Physics, Indian Institute of Technology Kharagpur, Kharagpur-721302, India

Corresponding Authors Email: [*]pkdatta@phy.iitkgp.ac.in, [$]utripathy@iitism.ac.in

1. Synthesis of Cz-PA complex

The 3-D view structure of the Cz-PA complex is represented in **Figure S1**.

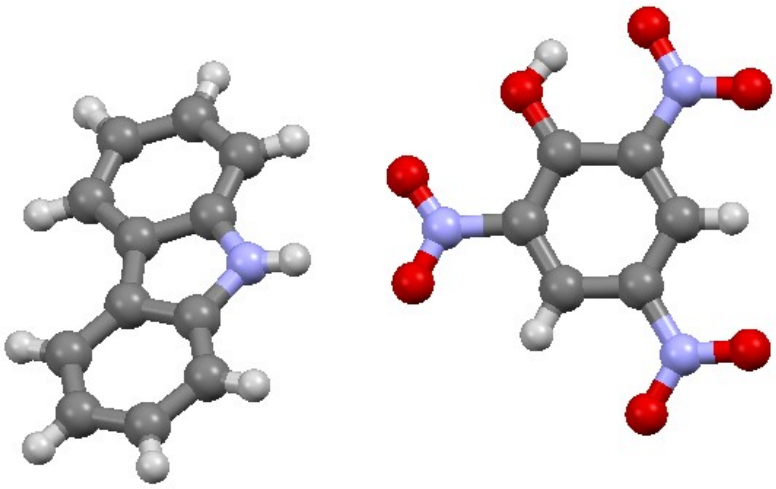

Figure S1. 3-D view of complex Cz-PA.

2. Single Crystal XRD (SC-XRD) analysis

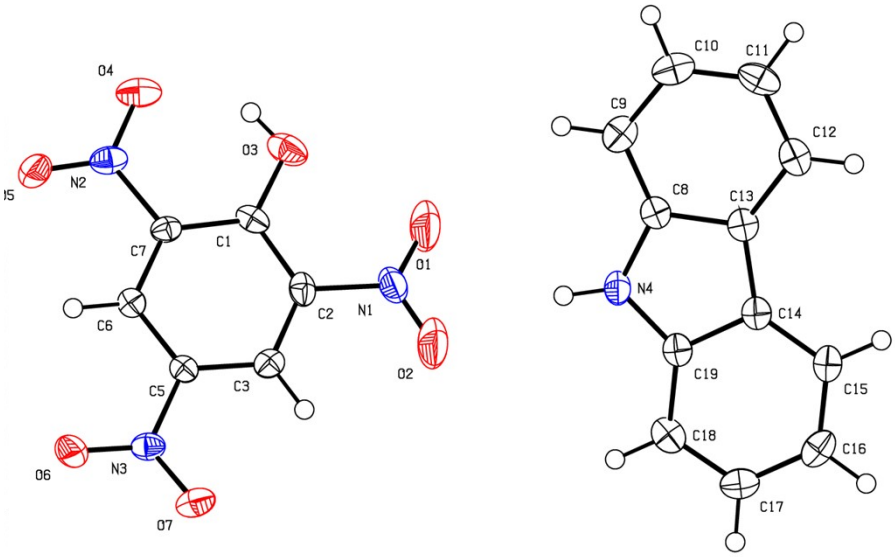

Figure S2. The ORTEP view plot of complex Cz-PA for crystal data.

Table S1. Anisotropic Displacement Parameters ($Å^2 \times 10^3$) for Cz-PA. The Anisotropic displacement factor exponent takes the form: $-2\pi^2[h^2a^{*2}U_{11}+2hka^*b^*U_{12}+\ldots]$.

Atom	U_{11}	U_{22}	U_{33}	U_{12}	U_{13}
O1	387(9)	50.9(17)	31.6(15)	43(3)	-2(3)
O2	387(9)	50.9(17)	31.6(15)	43(3)	-2(3)
O3	34.1(14)	21.6(13)	50.2(17)	2.7(12)	-12.2(14)
O4	36.6(15)	29.2(14)	47.9(17)	3.2(12)	1.6(13)
O5	51.2(18)	37.0(15)	23.6(13)	-8.6(14)	6.7(13)
O6	47.6(17)	22.8(13)	33.7(14)	5.5(13)	-9.4(13)
O7	34.6(15)	31.3(14)	32.7(14)	3.4(12)	-2.4(12)
N1	42(2)	27.7(16)	31.4(17)	-7.4(16)	-9.7(15)
N2	22.5(15)	26.8(16)	32.6(17)	-3.5(13)	2.1(13)
N3	20.8(14)	22.5(14)	29.1(15)	1.3(12)	-3.0(13)
N4	26.9(15)	28.7(16)	21.3(14)	-2.3(14)	-1.5(12)
C1	13.9(15)	16.9(15)	34.1(18)	-0.7(13)	-4.2(14)
C2	18.8(16)	28.5(19)	23.0(17)	-8.0(15)	-3.0(14)
C3	15.5(15)	26.4(17)	23.0(17)	-5.6(14)	-0.3(13)
C5	14.4(15)	19.0(15)	23.4(16)	-1.8(13)	-2.6(13)
C6	14.6(14)	21.7(16)	22.6(17)	1.9(13)	-2.1(13)
C7	17.4(15)	21.3(16)	22.9(16)	-3.0(14)	1.9(14)
C8	15.5(15)	25.5(17)	26.4(18)	2.3(15)	1.7(13)
C9	20.6(17)	40(2)	28.5(19)	-1.6(17)	1.9(15)
C10	21.5(18)	38(2)	39(2)	-1.4(17)	0.8(15)
C11	22.5(18)	21.5(18)	53(2)	6.7(16)	5.3(17)
C12	17.2(16)	30.7(19)	33.3(19)	2.6(15)	3.9(14)
C13	12.1(15)	27.4(17)	26.7(17)	1.4(14)	1.7(13)
C14	16.3(16)	26.7(18)	25.5(18)	4.3(15)	0.4(13)
C15	19.2(16)	33(2)	23.9(17)	3.8(15)	1.2(14)
C16	21.5(18)	43(2)	23.7(17)	8.6(16)	-0.1(14)
C17	18.5(16)	29.1(19)	36(2)	4.3(16)	2.8(15)
C18	16.3(16)	29.0(19)	37(2)	-1.2(14)	-1.3(15)

C19	16.1(16)	26.3(18)	25.5(17)	4.5(14)	0.2(13)

Table S2. Bond Lengths for Cz-PA.

Atom	Atom	Length/Å	Atom	Atom	Length/Å
O1	N1	1.144(5)	C5	C6	1.382(5)
O2	N1	1.141(5)	C6	C7	1.375(5)
O3	C1	1.323(4)	C8	C9	1.402(5)
O4	N2	1.246(4)	C8	C13	1.416(5)
O5	N2	1.205(4)	C9	C10	1.376(6)
O6	N3	1.233(4)	C10	C11	1.384(6)
O7	N3	1.226(4)	C11	C12	1.391(5)
N1	C2	1.458(4)	C12	C13	1.396(5)
N2	C7	1.464(4)	C13	C14	1.445(5)
N3	C5	1.460(4)	C14	C15	1.399(5)
N4	C8	1.377(5)	C14	C19	1.412(5)
N4	C19	1.384(5)	C15	C16	1.384(5)
C1	C2	1.410(5)	C16	C17	1.397(5)
C1	C7	1.410(5)	C17	C18	1.382(5)
C2	C3	1.386(5)	C18	C19	1.394(5)
C3	C5	1.380(5)			

Table S3. Bond Angles for Cz-PA.

Atom	Atom	Atom	Angle/°	Atom	Atom	Atom	Angle/°
O2	N1	O1	117.8(4)	C6	C7	N2	116.9(3)
C2	N1	O1	121.1(4)	C6	C7	C1	122.7(3)
C2	N1	O2	120.5(3)	C9	C8	N4	129.5(3)
O5	N2	O4	123.3(3)	C13	C8	N4	109.1(3)
C7	N2	O4	117.9(3)	C13	C8	C9	121.3(3)
C7	N2	O5	118.9(3)	C10	C9	C8	117.3(4)
O7	N3	O6	124.3(3)	C11	C10	C9	122.4(4)
C5	N3	O6	117.4(3)	C12	C11	C10	120.8(4)
C5	N3	O7	118.3(3)	C13	C12	C11	118.6(3)
C19	N4	C8	109.2(3)	C12	C13	C8	119.6(3)
C2	C1	O3	120.2(3)	C14	C13	C8	106.1(3)

C7	C1	O3	124.0(3)	C14	C13	C12	134.3(3)
C7	C1	C2	115.8(3)	C15	C14	C13	133.6(3)
C1	C2	N1	120.6(3)	C19	C14	C13	107.0(3)
C3	C2	N1	116.8(3)	C19	C14	C15	119.3(3)
C3	C2	C1	122.6(3)	C16	C15	C14	118.8(3)
C5	C3	C2	118.4(3)	C17	C16	C15	121.1(3)
C3	C5	N3	119.0(3)	C18	C17	C16	121.4(4)
C6	C5	N3	119.2(3)	C19	C18	C17	117.7(3)
C6	C5	C3	121.8(3)	C14	C19	N4	108.5(3)
C7	C6	C5	118.8(3)	C18	C19	N4	129.7(3)
C1	C7	N2	120.5(3)	C18	C19	C14	121.7(3)

Table S4. Hydrogen Atom Coordinates (Å×10^4) and Isotropic Displacement Parameters (Å^2×10^3) for Cz-PA.

Atom	**x**	**y**	**z**	**U(eq)**
H3	-4440(80)	-1246(16)	-3380.4(15)	53.0(10)
H4	-3837(4)	-1731(3)	-5475.7(10)	30.8(8)
H3a	-2979(5)	-5840(4)	-4445.6(12)	26.0(9)
H6	-3091(5)	-6072(4)	-2987.8(12)	23.5(8)
H9	-2639(5)	975(5)	-5034.7(13)	35.8(10)
H10	-1718(5)	3493(5)	-5215.2(15)	39.4(11)
H11	-1636(5)	4392(4)	-5998.1(15)	38.9(11)
H12	-2422(5)	2765(4)	-6643.8(13)	32.4(10)
H15	-3382(5)	140(4)	-7235.2(12)	30.4(10)
H16	-4224(5)	-2301(5)	-7521.9(13)	35.2(10)
H17	-4913(5)	-4311(4)	-6992.2(13)	33.6(10)
H18	-4735(5)	-3951(4)	-6159.0(14)	32.8(10)

3. Fourier-Transform Infrared (FTIR) Spectroscopy

Fourier-transform infrared (FTIR) spectra of the Cz-PA complex and its constituents are shown in **Figure S3** and **Figure 1(b)**. Generally, O-H, N-H, and C-H (aromatic) symmetric stretching vibrations are observed above 3000 cm^{-1} in the FTIR spectrum [1]. The observed shifts in characteristic bands, attributed to the stretching and bending vibrations of OH, NH, and CH functional groups in the FTIR spectrum of the complex, confirm crystal formation. These shifts result from intermolecular interactions, which are essential for the development of the crystal structure. A comparison of the FTIR spectra of the complex and its components reveals that the bands of the complex have shifted, indicating the influence of these intermolecular interactions [2]. In the FTIR spectrum of the complex, the peak at 3419 cm^{-1} is due to the O-H stretching vibration. The N-H stretching vibration is observed at 3346 cm^{-1}. The bands at 3086, 3078, and 3050 cm^{-1} appeared due to aromatic C-H symmetric stretching vibrations. C=C (aromatic) stretching vibrations are observed at 1651, 1630, 1610 and 1565 cm^{-1}. The peak at 1560 cm^{-1} is allocated for NO_2 (aromatic) asymmetric stretching vibration. The peaks at 1451 and 1435 cm^{-1} are assigned to C-H bending vibrations. The NO_2 symmetric stretching vibration is observed at 1364 cm^{-1}. The C-N stretching vibration is marked at 1335 cm^{-1}. The C-C stretching vibration is observed at 1240 cm^{-1}. The C-O stretching vibration is found at 1270 cm^{-1}. The peak at 1162 cm^{-1} is attributed to the C-H in-plane bending vibration. The observed peaks at 1108 and 704 cm^{-1} are found for N-H in-plane and out-of-plane bending vibration, respectively. The C-C-O stretching vibrations are marked at 1108 and 1080 cm^{-1}. The C-NO_2 stretching vibration is observed at 909 cm^{-1}. The peaks at 796 and 547 cm^{-1} are allocated for NO_2 wagging and rocking vibrations, respectively.

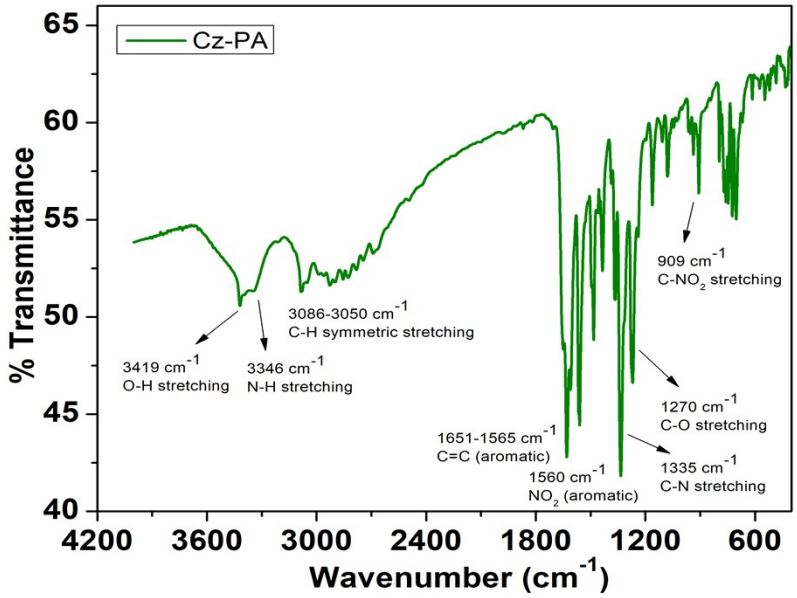

Figure S3. IR spectrum of Cz-PA complex.

4. Photophysical Study and UV-Vis Absorption Analysis

To investigate the photophysical properties of the Cz-PA complex, UV-Vis absorption spectral measurements of carbazole (Cz), picric acid (PA), and their complex (Cz-PA) were carried out using a UV/Vis spectrophotometer. The absorption characteristics provide insight into the electronic transitions within the materials, which are crucial for understanding their potential applications in optoelectronics and photonic devices. UV-Vis absorption spectra (shown in **Figure 2(a)**) of Cz, PA, and complex Cz-PA were recorded in ethanol at a concentration of 0.1 mM at room temperature in quartz cuvettes with a path length of 1 cm.

The absorption coefficient α_0 is a crucial parameter in understanding the optical properties of materials and can be calculated using the following relation

$$\alpha_0 = \frac{2.303 * A}{t}$$

or equivalently,

$$\alpha_0 = \frac{2.303 \log\left(\frac{1}{T}\right)}{t}$$

Where A is the absorbance, T is the percentage transmittance, and t is the thickness of the sample. Transmittance (T) is expressed as $T = 10^{-A} \times 100$.

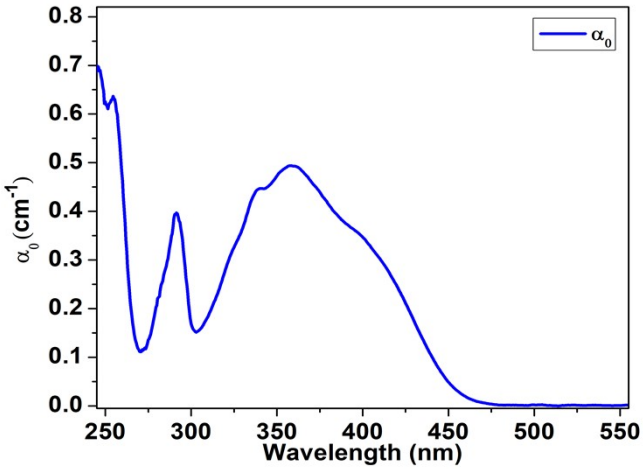

Figure S4. Variation of the absorption coefficient of Cz-PA complex with wavelength of light.

The variation of the absorption coefficient (α_0) with wavelength (shown in **Figure S4**) provides valuable insight into the interaction of light with the material. In **Figure S4**, the relationship between the absorption coefficient and the wavelength is illustrated, showing how (α_0) varies for the Cz-PA complex. This relationship is important for further understanding the optical band gap and the electronic transitions observed in the material. The absorption coefficient, $\alpha_0 = 0.15\ cm^{-1}$ is noted at the corresponding laser excitation of 520 nm for optical nonlinear calculations.

The optical band gap of the Cz-PA complex was determined using the Tauc relation [3], which is often applied to estimate the band gap of organic materials as follows

$$(h\nu\alpha_0)^2 = B(h\nu - E_g)$$

where α_0 is the absorption coefficient, $h\nu$ is the photon energy, E_g is the optical band gap, and B is a constant. The band gap of the Cz-PA complex, calculated from the absorption onset using a

Tauc plot is found to be 2.83 eV. This relatively low band gap indicates the potential of the complex for applications in optoelectronic devices where charge transfer interactions are crucial.

5. Ultrafast Optical Nonlinearity

Ultrafast Optical Nonlinearity was done using Z-scan setup (schematic shown in **Figure S5**) with femtosecond laser system. In this experiment, the sample was translated across the focal point using the motorized translated stage (GTS 150 Newport, USA) linked to a motion controller (ESP 301 Newport, USA). The transmittance beam was split using a beam splitter [90(T)/10(R)] in order to determine the CA and OA signals. A silicon photodiode (Thorlab, PDA100A, USA) was positioned behind a 1.5 mm aperture to detect the transmitted beam from the splitter to determine the CA signal, while another Si photodiode was used to collect the entire reflected beam in order to determine the OA signal. To prevent saturation, variable neutral density filters were positioned in front of both photodiodes. Two lock-in amplifiers (Signal Recovery 7225, AMETEK Scientific Instruments, USA) recorded the CA and OA signals in response to a 1 kHz transistor-transistor logic pulse generated by the pulse delay generator (SDG Elite, Coherent, USA). Another photodiode gathered a second reference signal reflected by a beam splitter placed in front of the laser system. A LabVIEW 2014 environment incorporated a motorized translational stage and lock-in amplifier for automation and data averaging.

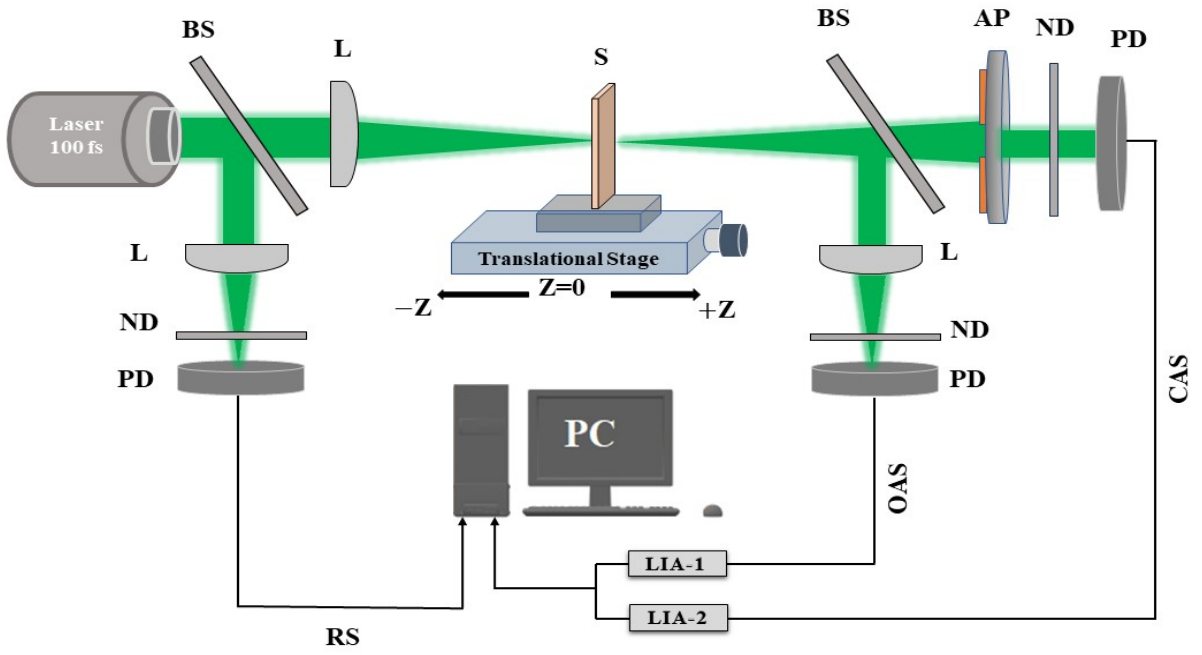

Figure S5. Z-scan setup for measurements of cubic optical nonlinearity (**BS:** Beam Splitter, **L**: Lens, **S**: Sample, **AP**: Aperture, **ND**: Neutral-density filter, **PD**: Photodiode, **LIA**: Lock-in amplifier, **CAS**: Closed-Aperture Signal, **OAS**: Open-Aperture Signal, **RS**: Reference Signal).

The peak intensity of the excitation laser (I_0) is determined via the following expression

$$I_0 = \frac{2 \times Average\ \ Power}{\pi w_0^2 \times\ Pulse\ Width \times Repetition\ Rate}$$

Where w_0 is the beam waist at the focus, $w_0 = 30\ \mu m$, Pulse Width = 100 fs, Repetition Rate = 1 kHz. For example, the computed peak intensity for an average peak power of 0.05 mW is 35 GW/cm^2.

In Z-scheme experiments, the coefficient of nonlinear refraction (n_2) is indirectly related to peak-valley transmittance change referred to as $\Delta T_{P-V} = 0.406(1-S)^{0.25}|\Delta\Phi_0|$, where the on-axis phase change $(\Delta\phi_0)$ at focus due to nonlinear refraction [4,5]. S is linear aperture transmittance, $S = 1 - exp(-2r_a^2/w_a^2)$ with aperture size (r_a) of 1.5 mm and laser beam size (w_a) at aperture.

The change in CA normalized transmittance of peak and valley (ΔT_{P-V}) (obtained from **Figure 3**) and the phase shift $(\Delta\phi_0)$ due to nonlinear refraction is also noted with the variation of peak intensity and given in **Table S5** and it signifies that the variation of ΔT_{P-V} with peak intensity increases due to large phase shifts (For the small aperture size, $\Delta\phi_0 \leq \pi$) at the higher peak intensity. Consequently, the nonlinear refraction becomes enhanced at higher peak intensity.

Table S5. Closed aperture Z-scan parameters for Cz-PA complex.

Peak Intensity GW/cm²	Δz_{P-V} **mm**	ΔT_{P-V} **a.u.**	$\Delta\phi_0$
35	09.15	0.342	0.915
57	10.15	0.801	1.863
85	10.47	1.022	2.995

Δz_{P-V}: Normalized transmittance peak-to-valley position separation,
ΔT_{P-V}: Change in normalized transmittance of peak and valley,
$\Delta\phi_0$: Phase shift due to nonlinear refraction

References

1 M. Raish, M. J. Alam, M. Mehkoom, Sultan, M. Ahmad, S. M. Afzal and S. Ahmad, *J. Mol. Struct.*, 2024, **1314**, 138713.

2 M. Raish, M. J. Alam, M. Ahmad and S. Ahmad, *J. Mol. Struct.*, 2023, **1290**, 135975.

3 J. Klein, L. Kampermann, B. Mockenhaupt, M. Behrens, J. Strunk and G. Bacher, *Adv. Funct. Mater.*, , DOI:10.1002/adfm.202304523.

4 M. Sheik-Bahae, A. A. Said, T. H. Wei, D. J. Hagan and E. W. Van Stryland, *IEEE J. Quantum Electron.*, 1990, **26**, 760–769.

5 T. Xia, D. J. Hagan, M. Sheik-Bahae and E. W. Van Stryland, *Opt. Lett.*, 1994, **19**, 317.